1262728

# THE UNITED STATES OF AMERICA

## TO ALL TO WHOM THESE PRESENTS SHALL COME:

**UNITED STATES DEPARTMENT OF COMMERCE**

United States Patent and Trademark Office

*December 16, 2004*

**THIS IS TO CERTIFY THAT ANNEXED HERETO IS A TRUE COPY FROM THE RECORDS OF THE UNITED STATES PATENT AND TRADEMARK OFFICE OF THOSE PAPERS OF THE BELOW IDENTIFIED PATENT APPLICATION THAT MET THE REQUIREMENTS TO BE GRANTED A FILING DATE.**

**APPLICATION NUMBER:** *60/456,190*
**FILING DATE:** *March 21, 2003*
**RELATED PCT APPLICATION NUMBER:** *PCT/US04/08345*

Certified by
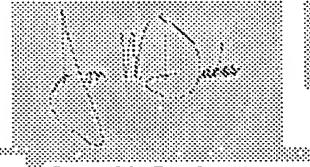
Jon W Dudas

Acting Under Secretary of Commerce
for Intellectual Property
and Acting Director of the U.S.
Patent and Trademark Office

11129 U.S. PTO 03/21/03

JC997 U.S. PTO 60/456190 03/21/03

# PROVISIONAL APPLICATION FOR PATENT COVER SHEET

This is a request for filing a PROVISIONAL APPLICATION FOR PATENT under 37 C.F.R. § 1.53 (c).

| Filing Date | March 21, 2003 | Docket No. | 4358-0113P |
|---|---|---|---|

| INVENTOR(s)/APPLICANT(s) | | |
|---|---|---|
| Given Name (first and middle (if any)) | Last Name | RESIDENCE (CITY AND EITHER STATE OR FOREIGN COUNTRY) |
| Hai-Wen | CHEN | Orlando, Florida, USA |
| Teresa L. | OLSON | Winter Garden, Florida, USA |
| Surachai | SUTHA | Kissimmee, Florida, USA |

☐ Additional inventors are being named on the _____ separately numbered sheets attached hereto

### TITLE OF THE INVENTION (280 characters max)

**POTENTIAL TARGET IDENTIFICATIN**

### CORRESPONDENCE ADDRESS

Birch, Stewart, Kolasch & Birch, LLP **or** Customer No. 2292
P.O. Box 747
· Falls Church

| STATE | VA | ZIP CODE | 22040-0747 | COUNTRY | U.S.A. |
|---|---|---|---|---|---|

### ENCLOSED APPLICATION PARTS (check all that apply)

| ☒ Specification | Number of Pages: 31 | ☐ Application Data Sheet. See 37 CFR 1.76. |
|---|---|---|
| ☒ Drawing(s) | Number of Sheets: 2 | ☐ Other (specify):_____ |

| METHOD OF PAYMENT (check one) | PROVISIONAL FILING FEE |
|---|---|
| ☐ Applicant claims small entity status. See 37 CFR 1.27. | ☐ Small Entity ($80.00) |
| ☒ A check or money order is enclosed to cover the Provisional filing fees. | ☒ Large Entity ($160.00) |
| ☒ The Commissioner is hereby authorized to charge filing fees and credit Deposit Account Number 02-2448, if necessary. | |

The invention was made by an agency of the United States Government or under a contract with an agency of the United States Government.

☒ No.

☐ Yes, the name of the U.S. Government agency and the Government contract number are:

Respectfully submitted,

BIRCH, STEWART, KOLASCH & BIRCH, LLP

Date: March 21, 2003

By _____
Michael K. Mutter, #29,680

P.O. Box 747
Falls Church, VA 22040-0747
(703) 205-8000

MKM/HNS/gf
4358-0113P

(Rev. 09/02/02)

# POTENTIAL TARGET IDENTIFICATION

It is advantageous to detect or identify image elements or targets as far away as possible. For example, in battle situations, candidate or potential
5   targets should be detected early, increasing the likelihood of an early detection of a target or other object. For a simple background scene such as a blue sky, a target may be recognized from a relatively long range distance. However, for some high clutter situations such as mountains and cities, the detection range is severely reduced. Moreover, such clutter situation are often complicated to
10   process. For example, the background may be mixed with different clutter types and groups. Also the background clutter may be non-stationary. In these types of situations, the traditional constant false alarm ratio (CFAR) detection technique often fails.

To solve the problems discussed above, spatio-temporal fusion
15   techniques is proposed for enhancing target detection (recognition). Several advanced detection schemes are proposed as well including a double-thresholding technique and a reverse-thresholing technique. These techniques may be applied to the complicated clutter situations where the traditional CFAR technique fails.

20   Also, pre-detection temporal integration and spatial fusion techniques are proposed for enhancing target detection and recognition. These techniques involve different spatio-temporal fusion strategies such as the additive, multiplicative, MAX, and MIN fusions. In spatial fusion, extracted features

from different sensors are fused. In temporal fusion, extracted features across a multiple time frame window are fused and integrated.

In addition, a double-thresholding technique is proposed when the background scene mixed with different clutter sub-groups. Some of them may

5 have means larger than the target mean, while some of them may have means smaller than the target mean. This technique selects a lower bound threshold (below the target mean) and a higher bound threshold (above the target mean). This technique in combination with the spatio-temporal fusion techniques will threshold out most of the different clutter groups.

10 Further, a reverse-thresholding technique is proposed when the background scene contains non-stationary clutters with increasing or decreasing means. The detection assignment criteria may be reversed depending on if the clutter mean is larger or smaller than the target mean.

The sensor clutter noise looking at real scenes (trees, grass, roads, and

15 buildings, etc.) has been studied. The sensor clutter noise at most (> 95%) of the sensor pixels is near stationary and un-correlated between pixels as well as (almost) un-correlated across time frames. The noise at a few pixels (looking at the grass near the road edge) has shown non-stationary properties (with increasing or decreasing mean across time).

20 If clutters with broader pdf (probability density function) than the target are encountered, it may be important to further investigate if the broad clutter pdf is caused by non-stationary noise with a time-variant mean or is caused by a mix of different clutter types with different stationary means. Then different

2

4358-0113 Provisional

detection techniques, such as the newly proposed double-thresholding or reverse-thresholding schemes, may be selected accordingly.

4358-0113P Provisional Application Attachment 01

## 1. INTRODUCTION

Spatio-temporal fusion for target classification is discussed. The fusion is conducted in *the likelihood function reading domain*. In general, the likelihood functions (pdfs) are obtained from training data based on single sensor and single frame measurements. Therefore, if we conducted fusion using the likelihood readings of the features extracted from measurements of single sensor and frame, we only need to store one set of likelihood functions for single sensor and frame, no matter how many sensors and frames we will use for fusion. On the other hand, since the detection process uses thresholding technique instead of likelihood functions, we can directly fuse the features values from different sensors and time frames in *the feature domain* for *target detection*.

Spatial fusion is defined as the fusion between different sensors, and temporal fusion is defined as the temporal integration across different time frames within a single sensor. Different spatial fusion and temporal integration (fusion) strategies have been developed and compared, including *pre-detection* integration (such as additive, multiplicative, MAX, and MIN fusions), as well as the traditional *post-detection* integration (the persistency test). The pre-detection integration is conducted by fusing the feature values from different time frames before the thresholding process (the detection process), while the post-detection integration is conducted after the thresholding process.

Although our techniques are aimed for improving target detection, these techniques can be used for other applications involving thresholding techniques. In target recognition, ATR (automatic target recognition) is a research area with high attention. One popular ATR approach uses the matched filtering/correlation techniques, and the resulting features after the correlation (e.g., the peak-to-sidelobe-ratio) will subject a threshold-screening to pick the recognized targets. Therefore, both the pre- and post-detection temporal integration methods can be used to enhance target recognition when multiple temporal frames are involved.

Temporal correlation and non-stationary properties of sensor noise have been investigated using sequences of imagery collected by an IR (256x256) sensor looking at different scenes (trees, grass, roads, buildings, etc.). The natural noise extracted from the IR sensor, as well as noise generated by a computer with Gaussian and Rayleigh distributions have been used to test and compare different temporal integration strategies. The simulation results show that both the pre- and post-detection temporal integrations can considerably enhance target detection by integrating only 3~5 time frames (tested by real sensor noise as well as computer generated noise). Moreover, the detection results can be further enhanced by combining both the pre- and post-detection temporal integrations.

## 2. SPATIO-TEMPORAL FUSION

For a physical sensor, the sensing errors are mainly caused by the measurement noise $n_m$ that is generally described as a RV (random variable)[1]. For target detection at the feature level[2], different features are extracted from the original physical measurements. The extracted features affected by the measurement noise are also RVs. The pdf (probability density function) of a feature RV may or may not have the same distribution as the original measurement noise[3]. To increase the Pd (probability of detection), we must reduce the influence of the feature RVs. The influence of RVs can be decreased by reducing the variances ($\sigma^2$) of the RVs and/or by increasing the distance ($d$) between the means of the two feature RVs related to the target and the clutter). The reduced feature variances and/or the increased feature distances will increase the signal-to-clutter-noise-ratio (SCNR) and thus lead to a better ROC (receiver operating characteristics) performance, i.e., a higher Pd for the same Pfa (probability of false alarms).

---

[1] For example, for an IR (infrared) sensor, the measurement noise (temporal noise) may be originated from scene-background, atmosphere transmission, path radiance, optics, filters, sensor housing and shield, detector dark current, pixel phasing, quantization, amplifier and read-out electronics, etc.

[2] In the IR sensor, for detecting a resolved target occupying multiple pixels and or a unsolved target occupying only a single target, a spatial matched filtering process in general is conducted before the detection (thresholding) process. The filter can be a Sobel edge extractor, a DOG (difference of Gaussian) filter, a specific tuned basis function, or an optical point spread function. The output of the filter is considered the feature values for detection.

[3] If a measurement noise has a Gaussian distribution and the extracted feature is a linear transform (e.g., the mean or average of multiple data points is a linear feature) of the physical measurement, the distribution of the feature RV will still be Gaussian. On the other hand, if the relationship between the extracted feature and the original measurement is non-linear, the feature distribution, in general, will be different from the original one. For example, for a radar sensor with a Gaussian distributed measurement noise, if we use the amplitude of the radar return real and imaginary signals as the extracted feature, the distribution of the feature RV will be Rayleigh.
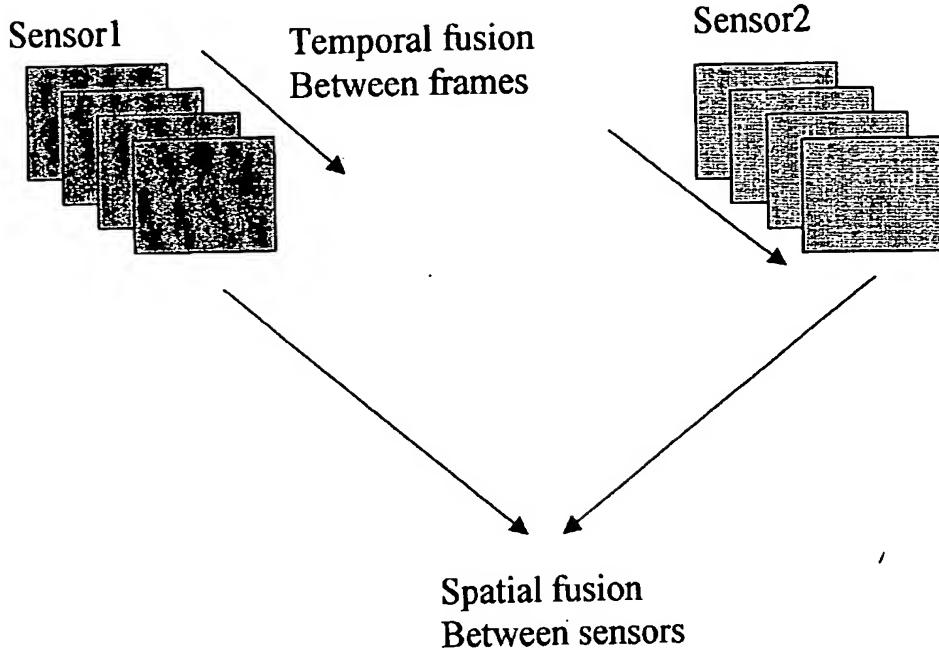
Figure 1. Spatio-temporal Fusion

Two approaches for reducing the variance of RVs are 1) temporal integration between time frames by averaging the RVs in different frames (the pre-detection integration), and 2) a binomial persistency test using a window of time frames (the post-detection integration). Wold in 1938 proposed and proved a theorem that gives us some insight into how temporal integration can be useful:

*Wold's Fundamental Theorem:*
*Any stationary discrete-time stochastic process {x(n)} may be expressed in the form*
$x(n) = u(n) + s(n)$,
*where u(n) and s(n) are uncorrelated process, u(n) is a RV, and s(n) is a deterministic process.*

Therefore, if u(n) is less temporally correlated, temporal integration will be more useful to reduce the variance of u(n). In this case, temporal integration across multiple time frames (temporal fusion) can enhance detection and classification results. The integrated spatio-temporal fusion is sketched in Fig. 1.

Besides the temporal uncorrelated noise condition that is important for effective temporal integration (fusion), there is another condition need to be addressed. In many realistic situations, the target may be moving and the sensor platform may be moving related to the background clutters. Therefore, another critical condition for effective temporal fusion is the accurate tracking and associating the targets and clutter objects (i.e., the detected objects) at different time frames using navigation initial tracker and/or image-based tracker or any effective image/object registration/association/correlation techniques.

## 3. DIFFERENT FUSION STRATEGIES

In this Section, we present four fusion (RV combination) strategies: 1) additive[4], 2) multiplicative, 3) MIN, and 4) MAX fusion.

### 3.1 Additive Fusion
The additive fusion rule for two sensors (or two time frames) is

---

[4] Please refer to [1] and [2] for more detailed description of the additive fusion and its advantage when adaptively weighting different sensors.

$$p(t) = p(t1) + p(t2), \quad \text{and} \quad p(c) = p(c1) + p(c2). \tag{1}$$

where $p(t)$ is the fused target feature values, $p(t1)$ and $p(t2)$ are the target feature values at sensor1 and sensor2 (or time frame1 and frame2), respectively; $p(c)$ is the fused clutter feature values, $p(c1)$ and $p(c2)$ are the clutter feature values at sensor1 and sensor2 (or time frame1 and frame2), respectively. In a frame, there are generally many more clutter feature values at different pixel locations.

The additive fusion can be easily extended to include more than two sensors (spatial fusion) or more than two time frames (temporal integration):

$$p(t) = p(t1) + p(t2) + \cdots + p(tn), \quad \text{and} \quad p(c) = p(c1) + p(c2) + \cdots + p(cn). \tag{2}$$

For two independent RVs: X and Y, the combined pdf of the summation of these two RVs ($Z = X + Y$) is calculated as the convolution of the two individual pdfs:

$$f_Z(z) = \int_0^\infty f_X(x) f_Y(z - x) dx. \tag{3}$$

In our additive fusion case (with two sensors or two frames), $p(t) = z$, $p(t1) = x$, and $p(t2) = y$ [or $p(c) = z$, $p(c1) = x$, and $p(c2) = y$]. From Eq. (3), we have

$$f_{p(t)}(p(t)) = \int_0^\infty f_{p(t1)}(p(t1)) f_{p(t2)}(p(t) - p(t1)) dp(t1), \tag{4}$$

and

$$f_{p(c)}(p(c)) = \int_0^\infty f_{p(c1)}(p(c1)) f_{p(c2)}(p(c) - p(c1)) dp(c1). \tag{5}$$

Eqs. (4) and (5) can be used to predict the detection performance of the additive fusion, since the ROC curves after the additive fusion can be estimated from the combined pdfs in Eqs. (4) and (5).

### 3.2 Multiplication Fusion
The multiplicative fusion rule of two sensors (or two time frames) is

$$p(t) = p(t1) * p(t2), \quad \text{and} \quad p(c) = p(c1) * p(c2). \tag{6}$$

For two independent RVs: X and Y, the combined pdf of the multiplication of these two RVs ($Z = X * Y$) is calculated as the nonlinear convolution (with divisions of a RV) of the two individual pdfs:

$$f_Z(z) = \int_0^\infty \frac{1}{|x|} f_X(x) f_Y(\frac{z}{x}) dx. \tag{7}$$

In our two-sensor multiplication fusion case, from Eq. (7), we have

$$f_{p(t)}(p(t)) = \int_0^\infty \frac{1}{|p(t1)|} f_{p(t1)}(p(t1)) f_{p(t2)}(\frac{p(t)}{p(t1)}) dp(t1), \tag{8}$$

and

$$f_{p(c)}(p(c)) = \int_0^\infty \frac{1}{|p(c1)|} f_{p(c1)}(p(c1)) f_{p(c2)}(\frac{p(c)}{p(c1)}) dp(c1). \tag{9}$$

### 3.3 The Relationship Between Additive and Multiplication Fusions

If we take the logarithm on both sides of the multiplication fusion equations [Eq. (6)], we have

$$ln[p(t)] = ln[p(t1)] + ln[p(t2)], \quad and \quad ln[p(c)] = ln[p(c1)] + ln[p(c2)]. \qquad (10)$$

The multiplication term becomes two additive terms of logarithm functions in each of the equation. If we have two RVs with log-normal pdfs, the equations above indicate that the multiplicative fusion of two RVs with log-normal distributions is equivalent to the additive fusion of two RVs with normal distributions.

### 3.4. MIN and MAX Fusions

The conjunction (AND) and disjunction (OR) are two frequently used combination rules in Fuzzy Logic. For two independent RVs: X and Y, the combined pdf of the conjunction of these two RVs [Z = min(X, Y)] is given as

$$f_Z(z) = f_X(z)[1 - F_Y(z)] + f_Y(z)[1 - F_X(z)], \qquad (11)$$

where $F(z)$ is the cumulative distribution function.

Similarly, for two independent RVs: X and Y, the combined pdf of the disjunction of these two RVs [Z = max(X, Y)] is given as

$$f_Z(z) = f_X(z)F_Y(z) + f_Y(z)F_X(z). \qquad (12)$$

For our two-object problem, the MIN (conjunction) fusion is

$$p(t) = min[p(t1), p(t2)], \quad and \quad p(c) = min[p(c1), p(c2)]. \qquad (13)$$

The MAX (disjunction) fusion is

$$p(t) = max[p(t1), p(t2)], \quad and \quad p(c) = max[p(c1), p(c2)]. \qquad (14)$$

The terms of pre- and post-detection integrations were originally used in radar sensor detection. They can be equally applied for IR sensor detection. For both methods, a temporal moving integration widow (typically containing several frames, e.g., N = 5 or 7) is first selected. In the pre-detection method, one of the different fusion strategies (discussed in the last section) is applied for the frames within the window size. The fused features values are then used for detection (applying thresholding). In the post-detection (also called persistency test) method, detection (thresholding) is first performed on each image frame within the moving window (with N frames). Then evaluate how many detections out of the N frames occur for a detected object. For example, for a criteria of 5-out-of-7, if an object was detected from 5 or more frames in a moving window with 7 frames, the detected object is considered as a target. Otherwise, it is considered as noise or clutter detection.

## 4. PRE- AND POST-DETECTION TEMPORAL INTEGRATION
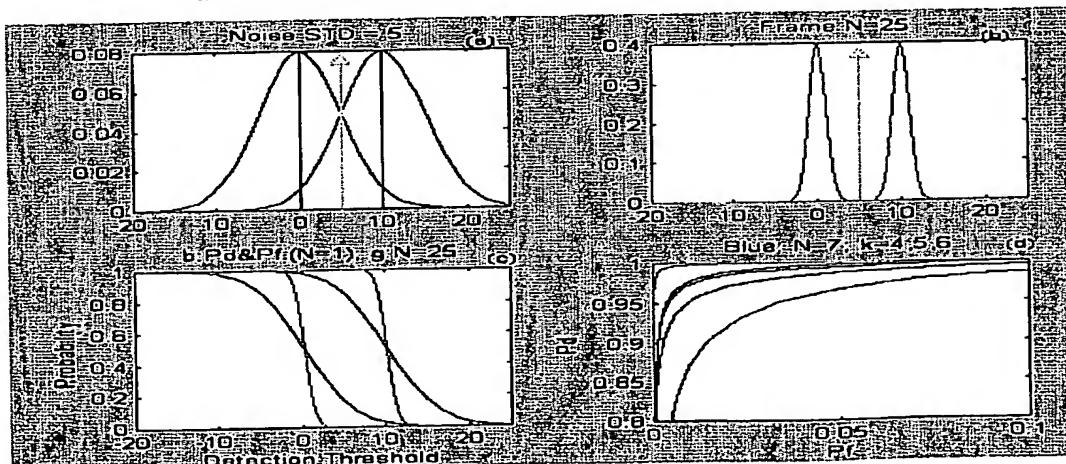
**Figure 2. ROC Performances of Pre- and Post-Detection Integration**

Fig 2(a) shows the pdfs (probability density functions) for a noise and a target in a single frame with STD (standard deviation) = 5. Fig 2(b) shows the pdfs after averaging 25 frames (the pre-detection integration: equivalent to the additive fusion). The accumulated probability curves (the erf functions) of the pdfs in Fig 2(a) and (b) are plotted in Fig 2(c) (Blue curves: the single frame; Green curves: average of 25 frames). Several ROC curves are plotted in Fig 2(d)[5]. The top and bottom (red) curves are 7-frame average and 3-frame average, respectively. The middle three (blue) curves are 4-out-of-7, 5-out-of-7, and 6-out-of-7 persistency test results.
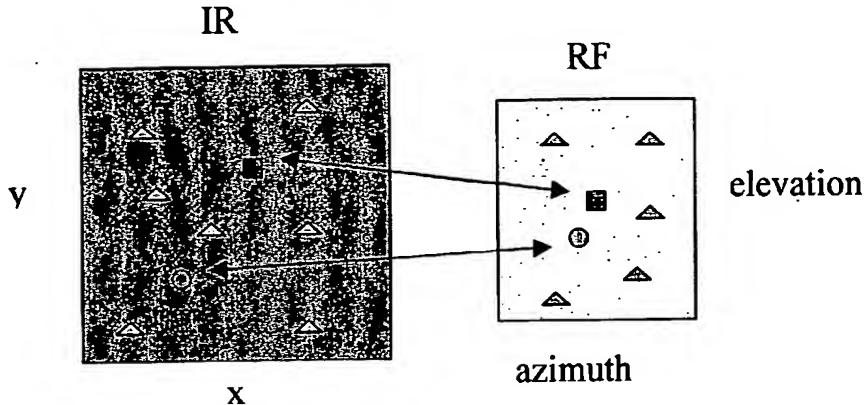


**Figure 3. Target Detection under a Two-target Situation**
Square: target1; Circle: target2; Triangle: clutter noise

## 5.  SIMULATIONS OF TARGET DETECTION

As shown in Fig 3, we simulated both IR and RF sensors for target detection enhancements using spatio-temporal fusion. Spatial Fusion (integration) is conducted between the IR and the RF frames (pre-detection integration only), while Temporal Fusion is conducted across several time frames of each sensor (both pre- and post-detection integration). Two target situations were simulated: 1) single-target in the scene, and 2) two-targets in the scene. In general, the single-target case has less adjustable parameters and thus would be easier to compare performances from different fusion strategies than the multiple-target case. However, the multiple-target case occurs at many realistic situations. A two-target case is shown in Fig 3. In this simulation, we used static targets and clutter, and presume perfect object tracking and/or registration across multiple time frames.
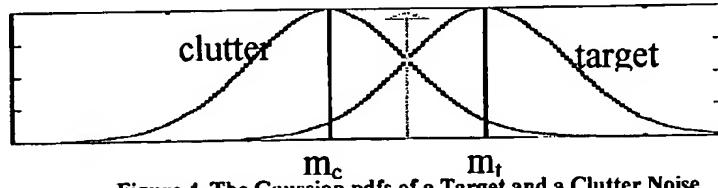


**Figure 4. The Gaussian pdfs of a Target and a Clutter Noise**

50 random data samples (related to 50 time frames) were generated as performance data set for each object (target or clutter noise) to evaluate the detection performance. The detection was conducted using the traditional CFAR (constant-false-alarm-ratio) strategy. For a specific CFAR threshold, each detected target at one of the 50 frames counts on 2% of Pd (probability of detection) for the single-target case, and 1% of Pd for the two-target case. The noise in IR is simulated as a normal distribution with a standard deviation of 10, and the noise in RF is simulated as a Rayleigh distribution with

---

[5] For the pre-detection integration, the ROC curves are obtained by directly plotting the accumulated probability curves in Fig 2(c) as the x- and y-axis in Fig 2(d). For a k-out-of-N post-detection integration, the accumulated probability curves need to be transferred to post-detection accumulated probability curves using the binomial equation: $P(k:N) = \sum_{j=k}^{N} \binom{N}{k} p^{j} (1-p)^{N-j}$

a standard deviation of 6.5. Fig 4 shows the pdfs (probability density functions) of a target and a clutter noise with normal distribution.

The detection ROC performances without any temporal integration (single frame) are shown in Fig 5 as a baseline performance to compare different temporal fusion strategies. Fig 5(a) shows the baseline result from an IR sensor, while Fig 5(b) shows that from a RF sensor. The y-axis is the Pd (probability of detection), and the x-axis is the false-alarm number per frame. The curve with circle symbols is the result from the single-target case, and the curve with square symbols is the result from the two-target case. It is seen that for a false alarm rate of two false alarms per frame the Pd is about 80% for IR and 85% for RF, and that the single-target case performs a little better that the two-target case.
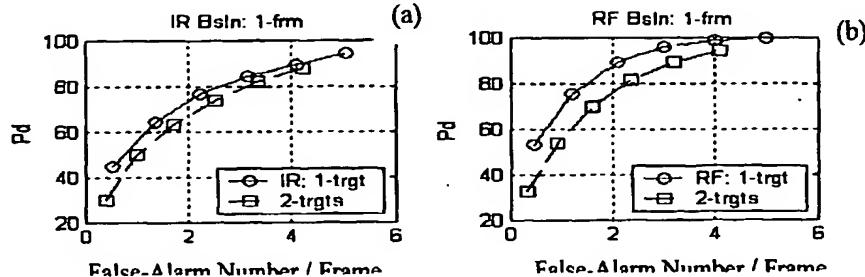


Figure 5. The Baseline (Single Frame) Detection ROC Performance
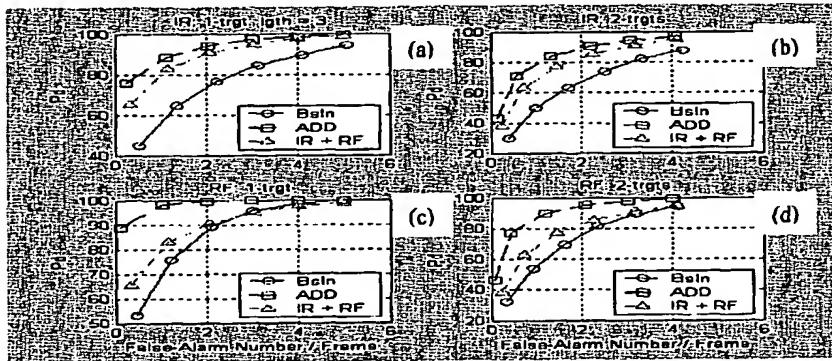


Figure 6. Additive Spatio-Temporal Fusion (Window = 3 frames)
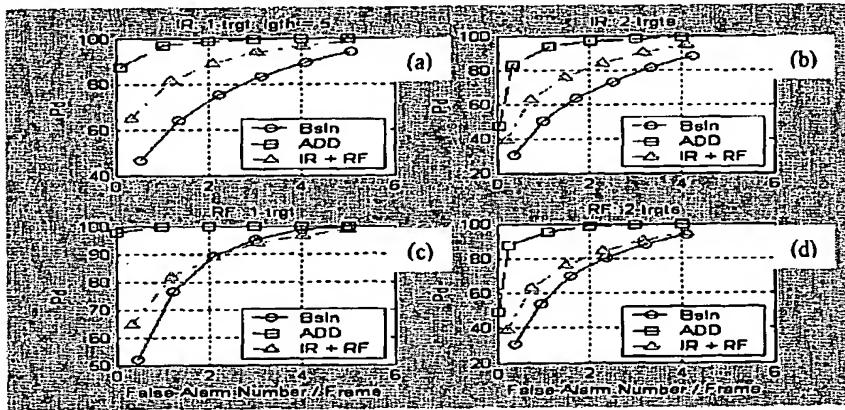


Figure 7. Additive Spatio-Temporal Fusion (Window = 5 frames)

**5.1 Additive Spatial Fusion vs. Additive Temporal Fusion**

For the four different fusion strategies discussed in Section 3, our simulation results for target detection show that the multiplication fusion performs the same as the additive fusion, and the MIN fusion performs a little better than the MAX fusion. In this paper, we show the results for the Additive and MIN fusion.

The detection ROC performance curves for the single-target case of IR sensor are shown in Fig 6(a), while the detection ROC performance curves for the two-target case of IR sensor are shown in Fig 6(b). The curve with the circle symbols shows the baseline performance (single frame). The curve with the triangle symbols shows the result of spatial additive fusion between the IR and the RF sensor, while the curve with the square symbols shows the result of additive temporal fusion by integrating a time window of three frames. Similar results for the RF sensor are shown in Fig 6(c) and (d). It is found: 1) the spatial fusion enhance the detection than the single sensor along, although the IR (the worse sensor) enhanced more than the RF (the better sensor) did; 2) The temporal fusion using three time frames performs better that the spatial fusion using only two sensors. In general, if the noise in different frames are independent to each other, a temporal fusion with N (=2,3,...) frames should perform similar to a spatial fusion with N sensors. We will discuss the noise correlation properties between frames in a later section. The results of additive temporal fusion using five time frames are shown in fig 7. It is seen that the target detection can be further enhanced by increasing the time window of integration.

## 5.2 Additive Temporal Fusion vs. MIN Temporal Fusion
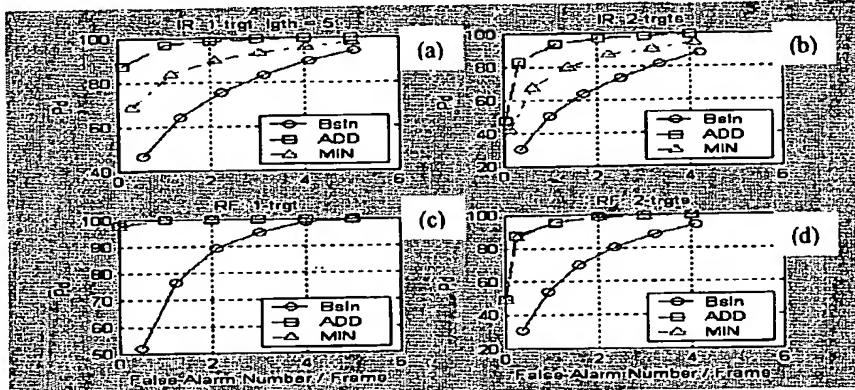


Figure 8. Additive and MIN Fusions (Window = 5 frames)

The results comparing the additive fusion with the MIN fusion for an integration window of five frames are shown in Fig 8. Both additive and MIN fusions with multiple frames enhance target detection. For the IR sensor (with normal noise distribution), the additive fusion always outperforms the MIN fusion in both the single-target and two-target cases as shown in Fig 8(a) and (b), while for the RF sensor (with Rayleigh noise distribution), the MIN fusion can further enhance target detection, and performs equally well as the additive fusion in both the single-target and two-target cases as shown in Fig 8(c) and (d).
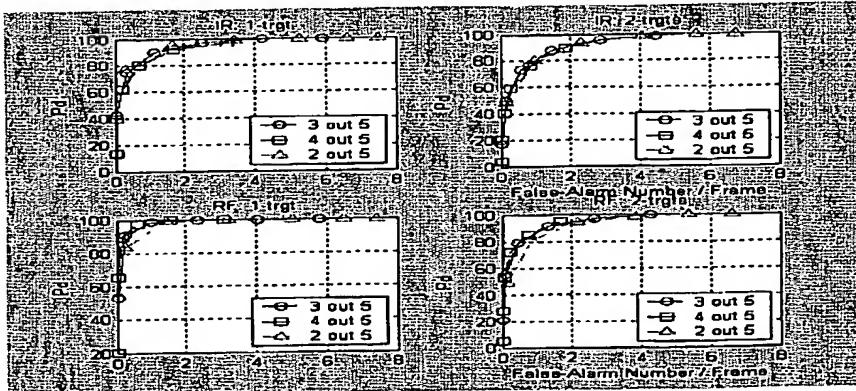
**Figure 9. Persistency Test (Window = 5 frames)**
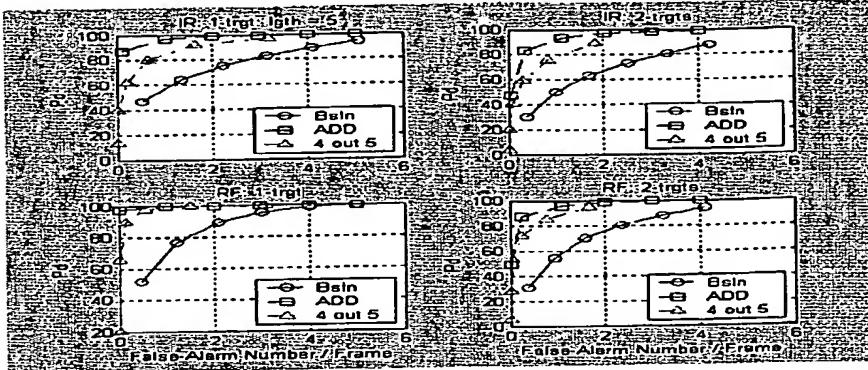
**Figure 10. Additive Fusion and Persistency Test (Window = 5 frames)**
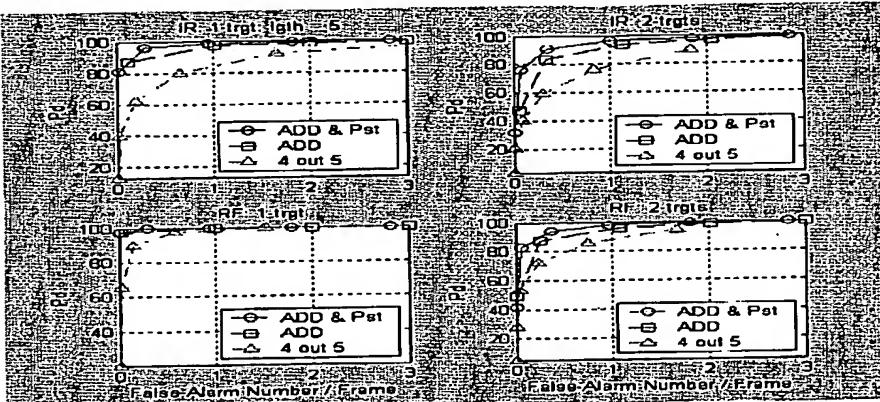
**Figure 11. Combination of Additive Fusion and Persistency Test**

### 5.3 Post-Detection Integration (Persistency Test)

The persistency test has been discussed and shown in Section 4 and Fig 2. Persistency test results for both IR and RF sensors are shown in Fig 9. The three curves in each figure are the persistency test for K out of N frames (K=2,3,4; and N=5). Similar to the result in Fig 2(d), the three curves in Fig 9 show similar detection enhancements.

### 5.4 Additive Fusion vs. Persistency Test

Figure 10 shows the results of additive fusion (the curve with square symbols) and the persistency test (the curve with triangle symbols) for both the IR and RF sensors. It is found from Fig 10 that by integrating only five frames, both additive fusion and persistency test can significantly enhance target detection from the baseline (single frame), with additive fusion performing a little better than the persistency test.

Furthermore, the additive fusion and the persistency test can be complementary to each other. They can be combined to further enhance target detection. Results using an integration window of five frames are shown in Fig 11. The curves with triangle symbols show the ROC performance of the persistency test, the curves with square symbols show the ROC performance of the additive fusion, and the curves with circle symbols show the combination ROC performance of the additive fusion and persistency test.

## 6. TEMPORAL CORRELATION PROPERTIES OF REAL IR NOISE

As discussed in the previous section, the performance of temporal integration depends on the temporal correlation properties of the sensor noise. The better performance can be achieved if the noise across the time frames is less correlated. In the simulate results presented in the previous section, we used computer generated random noise that is generally uncorrelated between frames. What about the real sensor noise? To answer this question, we extracted and
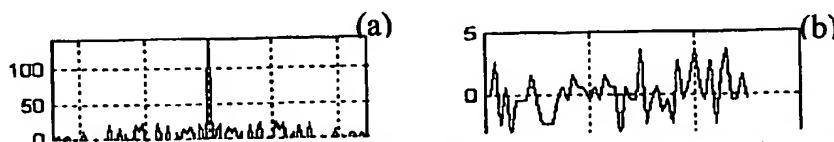
studied the multiple frame noise from an *InSb* IR FPA (focal plane array) with 256x256 pixels. Imagery sequences (50 time frames) were collected by this IR sensor looking at different scenes (trees, grass, roads, buildings, etc.).

**Figure 12. Auto-correlations of Real and Computer Generated Noise**
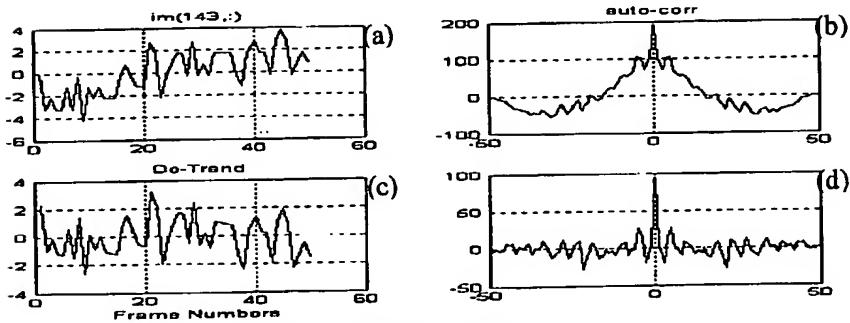


**Figure 13. Noise De-trend**

Studies of the natural IR noise have revealed that 1) the sensor noise at most (> 95%) of the sensor pixels are near stationary and un-correlated between pixels as well as (almost) un-correlated across time frames; and 2) the noise at a few pixels (e.g., the grass aside the road) has shown non-stationary properties (with increasing or decreasing mean across time). Fig 12(b) shows a typical stationary and uncorrelated noise sequence (50 frames) from a specific pixel. Its auto-correlation function is shown in Fig 12(a). Fig 12(d) shows a typical non-stationary noise sequence with a decreasing mean across time. Its auto-correlation function with high temporal correlation is shown in Fig 12(c). Fig 12(e) shows the auto-correlation function of a Gaussian random noise sequence (50 frames) generated by a computer (this noise has been used in the simulation discussed in the previous section). It is seen that the natural noise and the computer-generated noise have similar auto-correlation functions [Fig 12(a) and (e)], and thus both are highly uncorrelated across time.

From the natural IR noise, we notice that the non-stationary noise at a specific pixel always shows high values off the center peak in the correlation function. To understand whether the high vales caused by the non-stationary properties only, or caused by both non-stationary and temporal correlation, we have de-trended the non-stationary noise sequences, and remove the increasing or decreasing means. Then we found that the de-trended noise (becoming a stationary process) becomes temporally uncorrelated (low values off the center peak in the correlation function). This finding indicates that the noise at pixels with high off-center correlation values is non-stationary but not temporal correlated. One such example of the noise de-trend is shown in Fig 13. Fig 13(a) shows a non-stationary noise sequence with a increasing mean whose auto-correlation function is shown in Fig 13(b). Fig 13(c) shows the same noise after de-trend process, and its auto-correlation function is shown in Fig 13(d). It is seen that the auto-correlation function in Fig 13(d) has much lower off-center-peak values than that in Fig 13(b).

9

We have applied the IR real noise to test our different temporal fusion strategies, as well as pre- and post-detection temporal integration. The performances using the stationary IR noise are similar to the performances using computer-generated noise as shown in the previous section. Fig 14(b) shows a stationary target noise sequence (50 frames, the solid curve) and a stationary clutter noise sequence (the dashed curve). The target detection ROC performances are shown in Fig 14(a). The curve with circle symbols shows the baseline (single frame) performance. The curve with triangle symbols shows the performance using persistency test with an integration window of 3 frames (2 out of 3), and the curve with square symbols shows the performance of additive fusion with an integration widow of 3 frames. Fig 14(d) shows a non-stationary target noise sequence (the solid curve) with a decreasing mean and a stationary clutter noise sequence (the dashed curve). The target detection ROC performances are shown in Fig 14(c). It is seen that the detection performances are much worse than the results shown in Fig 14(a).
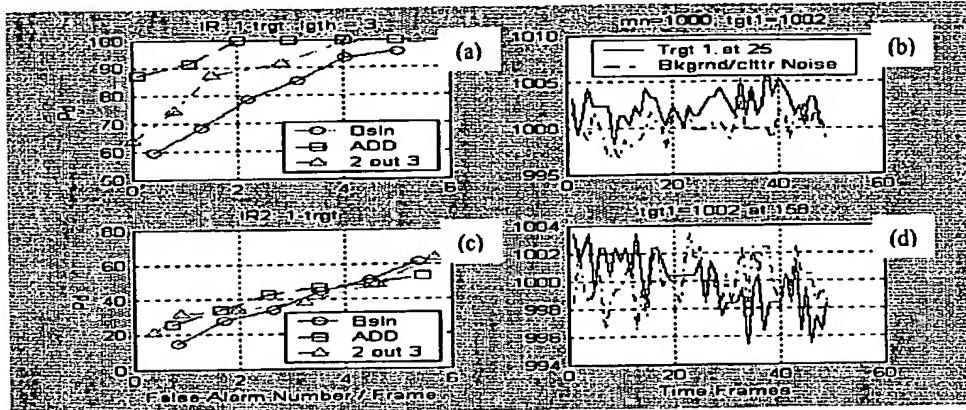


Figure 14. Target Detection Using Real IR sensor Noise

## 7. DISCUSSION AND SOME FURTHER THOUGHTS

### 7.1 Temporal Fusion and IR Sensor Non-Uniformity Correction

In the traditional NUC (non-uniformity correction) design, frame subtraction is generally used to subtract out the FPN (fixed pattern noise). However, direct subtraction of two adjacent frames will double the variance of the temporal noise. To avoid a large increase of temporal noise, the NUC design is applied a feedback loop and only a small fraction of the FPN is subtracted out at each iteration. Nevertheless, if we apply temporal integration in the detection system after the NUC process, we can afford the direct subtraction between two nearby frames, and further reduce the noise. For example, the sum of $n$ original frames results in a variance of $n \times v$ (where $v$ is the single frame variance). On the other hand, the sum of $n$ subtracted frames results in a variance of $2 \times v$, because all the variances in the middle frames are cancelled out and only the two variances in the first and the last frames are leftover. Therefore, for an average of $n$ original frames, the resulting variance is $v / n$, while averaging $n$ subtracted frames, the resulting variance is $4v / n^2$. That is, $(4v / n^2) < (v / n)$ when $n > 4$.
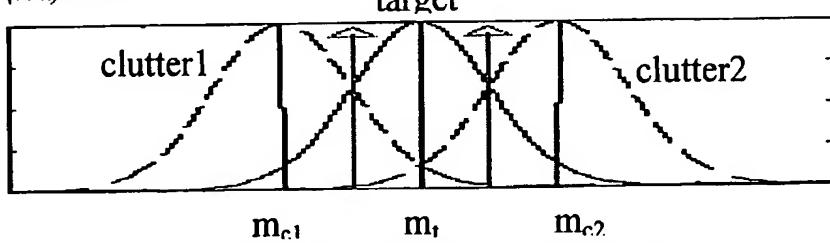


Figure 15. Gaussian pdfs of Clutters and Target

### 7.2 Double-Thresholding Detection Scheme

If the feature values of all different clutters in a scene are lager (or smaller) than the target feature value as indicated in Fig 4, the traditional *CFAR detection scheme* will still works. For the example in Fig 4, the CFAR scheme always treats an object with a feature value below the threshold as a clutter, and above the threshold as a target. However, in

reality, the clutter situations are very complicated. As shown in Fig 15, some clutter groups (e.g., some trees or roads) may have feature values lower that the target, while some other clutter groups (e.g., some decoy-like objects, or counter-measurement objects) may look more like the target and thus have feature values higher than the target. In these situations, the traditional CFAR scheme will partly fail because it only uses a single-thresholding scheme that can only threshold out one of the clutter group and left the other to be more likely false detected as a target.

In the situation that some clutter feature values are larger than and some are smaller than the target feature value, we propose a *double-thresholding scheme* with one up-bound threshold and one lower-bound threshold. The technique in combination with the temporal integration will considerably enhance target detection. For example, as shown in Fig 15, suppose the two clutters and the target have Gaussian distributions with the same variances. The separation of the target from the two clutters is two σ (i.e., two standard deviation):

$$m_t - m_{c1} = m_{c2} - m_t = 2\sigma$$

If we set the double thresholds as one σ below and one σ above the target mean $m_t$, the detection criteria is that only a object with a feature value larger than the lower bound threshold and smaller than the higher bound threshold is assigned as a detection. This is a two-sigma probability and for a Gaussian distribution the Pd (Probability of target detection) is around 68%, and the Pfa (probability of false-alarm) caused by the two clutter groups is around 34% (= 17% + 17%). This is the baseline performance for the traditional single frame detection. However, if we apply the temporal integration of 9 frames[6] with the additive fusion (equivalent to averaging 9 frames), the standard deviations for the clutters and the target will be reduced by a factor of 3. Then this is a six-sigma probability. The Pd is increased to above 99%, and the Pfa caused by the two clutters is reduced to below 2%.

In this technique, for appropriately selecting the two thresholds, we prefer to have the pre-knowledge of the target mean that may be available from some good training data.

### 7.3 Reverse-Thresholding Detection Scheme

Another situation that the traditional CFAR scheme will fail is when non-stationary targets and/or clutters exist. As shown in Fig 14(d) where a non-stationary target with a decreasing mean exists. At an earlier time moment, the target mean is larger than the clutter mean, while at a later time moment the target mean is below the clutter mean. For a traditional CFAR single-thresholding approach, we set a single threshold[7], and any object with a feature value above it will be assigned as a detected target. This approach work at earlier time moments when the target mean is larger than the clutter mean. However, it will fail when the target mean moves close to and further below the clutter mean, the clutter will have much higher probability to be falsely detected as a target than the real target. That is why the detection performances in Fig 14(c) are much worse that those in Fig 14(a).

Similarly, a non-stationary clutter situation can be easily understood using Fig 15. Suppose at an earlier moment the non-stationary clutter with a increasing mean was at the clutter1 location. At a later time moment, it moved from the left-side of the target to the right-side of the target at the clutter2 location. Based on these observations, we propose a *reverse-thresholding scheme* to deal with the non-stationary case. As shown in Fig 15, when the non-stationary clutter mean is blow the target mean, we set the criteria for assigning a detection as the object's feature value is above the threshold, while when the clutter mean changed to above the target mean, we set the criteria for assigning a detection as the object's feature value is below the threshold. This technique needs the real time measurements of the changing mean of a non-stationary process. This task may be conducted by using a temporal moving widow or the Wiener and/or Kalman filtering techniques.

## 8. SUMMARY

1). Both the pre- and post-detection temporal integrations considerably enhance target detection by integrating only 3~5 time frames (tested by real sensor noise as well as computer generated noise).

2). The newly developed pre-detection temporal integration techniques (Additive, Multiplicative, or MIN Fusion) perform a little better than the traditional post-detection temporal integration technique (Persistency Test). Detection results can be further enhanced by combining both the pre- and post-detection temporal integrations.

---

[6] Presume that the noise in the frames is temporally un-correlated.

[7] Note: for the traditional CFAR scheme, the threshold itself is changing (floating) from frame to frame to keep a constant false-alarm rate.

3). The techniques developed in this study can be further used for target recognition such as the ATR using matched filtering/correlation approach.

4). The sensor clutter noise looking at real scenes (trees, grass, roads, and buildings, etc.) has been studied. The sensor clutter noise at most (> 95%) of the sensor pixels is near stationary and un-correlated between pixels as well as (almost) un-correlated across time frames.

5). The noise at a few pixels (looking at the grass near the road edge) has shown non-stationary properties (with increasing or decreasing mean across time).

6). Based on observations over the real IR sensor clutter noise, we proposed two advanced thrsholding techniques: the double-thresholding and the reverse-thresholding. They can outperform the traditional CFAR single-thresholding technique when involving complicated clutter situations.

7). From the training data, if we encounter clutters with broader pdf (probability density function) than the target, it would be important to further investigate if the broad clutter pdf is caused by non-stationary noise with a time-variant mean or is caused by a mix of different clutter types with different stationary means. Then we can accordingly select different detection techniques such as the newly proposed double-thresholding or reverse-thresholding schemes discussed in the previous section.

8). It's critical to further investigate and understand the non-stationary noise property under different weather conditions and different background scenes and textures such as grass, trees, sand, and water surfaces, etc.

**4358-0113P Provisional Application Attachment 02**

## 1. INTRODUCTION

For an IR (infrared) sensor, the raw digital images coming out from the FPA (focal plane array) A/D converter contain strong non-uniformity/fixed pattern noise (FPN) as well as permanent and blinking dead pixels. Before performing the target detection and tracking functions, these raw images are processed by a CWF (chopper-wheel-free) MBPF NUC (Measurement-Based-Parametric-Fitting Non-Uniformity Correction) system to replace the dead pixels and to remove or reduce the FPN, as shown in Figure 1. The input to MBPF NUC is $RIM_{i,j}$ (the raw image), where $1 \leq i, j \leq 256$, and the output is $CIM_{i,j}$, the corrected image. It is important to note that as shown in Figure 1 the IT (integration time) for the FPA input capacitors is a critical parameter to control the sensor's sensitivity and temperature DR (dynamic range).

From the results of our FPN measurement, the STD (standard deviation) of FPN from a raw uncorrected image can be as high as 300-400 counts. This high count FPN will severely reduce the sensor's sensitivity (we would like to detect a weak target as low as a couple of counts) and hamper the target tracking and/or ATR functions because of the high counts FPN artifacts. Therefore, the major purpose of the NUC system is to reduce FPN for early target detection, and the secondary purpose is to reduce FPN artifacts for reliable target tracking and ATR.



$$V_p = \frac{1}{C} \int_0^{t_{int}} I_p \, dt = \frac{I_p}{C} t_{int}$$
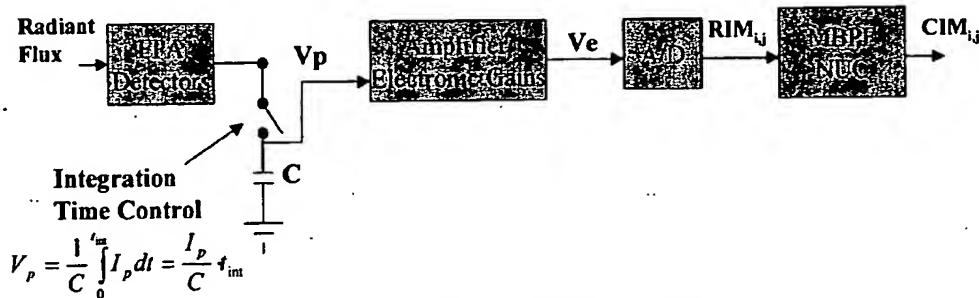
**Figure 1 FPA & NUC System**

The CWF MBPF NUC system we have developed contains three functions: 1) Permanent and blinking Dead Pixel Replacement (PBDPR), 2) Temperature Dynamic Range Management (DRM), and 3) FPN Estimation and Removal (FPN E&R).

The PBDPR function is to replace the permanent and blinking (deviant) dead pixels using some global and/or local thresholding techniques. The input to this function is $RIM_{i,j}$, and the output of this function is $DPR_{i,j}$.

The DRM function is designed for the system to optimally satisfy the requirement of the temperature dynamic range as well as the system sensitivity (detectivity) requirements. Different ITs (integration times) and electronic gains are assigned to different temperature sub-dynamic ranges (sub-DRs). The input to the DRM function is $DPR_{i,j}$, and the output of the DRM function is $DRM_{i,j}$.

The FPN E&R function is to estimate and reduce the FPN based on laboratory measurements. Piece-wise (2 pieces) or one-piece linear curve fittings are used for different sub-DRs to estimate the FPN at different temperatures and ITs (integration times). The input to the FPN E&R function is $DRM_{i,j}$, and the output of the FPN E&R function is $CIM_{i,j}$. Figure 2 shows the algorithm flow diagram for the MBPF NUC system with the three functions.

1

**Functions:**

| | | |
|---|---|---|
| Global & Local Thresholding; Temporal variance Test, etc. | For Temp > 70 deg C, IT = 2.5 ms, GE = low. For Temp: 35~70 deg C, IT = 5.2 ms, Ge = low. For temp 0~35 deg C, IT = 9 ms, Ge = low. For temp –33~0 deg C, IT = 16.6 ms, Ge = low. | Using piece-wise (2 pieces) Linear curve fitting for the middle and high Sub-DRs; Using one-piece linear curve fitting for the low and very high sub-DRs. |

**Figure 2 Algorithm Flow Diagram of MBPF NUC**

As shown in Figure 2, the DRM is a subsystem in a NUC system. The DRM, like the automatic gain control in a radio system, adaptively adjusts the IT (integration time) of the FPA to meet the requirements of both the sensor sensitivity and operating temperature dynamic range. The DRM also handles the pixel-saturation problem by reducing the IT. In the traditional NUC design (the prior art) using a chopper-wheel (or blurring/deformable lenses), the DRM frequently switches the ITs to keep the pixel intensity at the middle-intensity -counts (the half quantum well) to avoid the pixel starvation and saturation situations. There are three problems with this design:

1) . The frequent changes of IT will vary the sensor sensitivity and also need more processing power.
2) In many applications of IR measurements, we want to know the objects' radiant intensity from the measured object irradiance (for example, in the Missile Defense Program the radiant intensity is a critical physical feature for target discrimination and classification). However, the calibration for estimating the radiant intensity is related to each operating IT. Therefore, in this case we would like to use a few operating ITs instead of changing ITs frequently with many different values.
3) If the target pixels are saturated then it is okay to reduce the IT, however, if the saturation pixels are from some uninteresting objects, clutters, or from some burning CM (counter-measurement) objects, and if the target signature is still weak, we would not want to reduce the IT.

In general, the CWF NUC prefers to use a small number of operating ITs so that it does not require a large number of coefficients for estimating the FPN. In this DRM design, we pre-select a few ITs (four ITs in this design) depends on the requirements for sensitivity and dynamic range, and the DRM will smartly and adaptively choose the appropriate IT depending on the background temperatures and pixel-saturation situations. Based on our lab measurements, four integration times (2.5, 5.2, 9, and 16.6 ms) have been selected for the DRM to meet the requirements for both the seeker sensitivity and temperature dynamic range. The basic and advanced logic functions have been developed for the DRM.

We first decide the three IT-switching temperatures (0, 35, and 70 deg C). The decision is based on several facts that (i) longer IT leads to lower NEDT, shorter DR, and more image blurring caused by motion; (ii) preferring to operate at the linear region of the sub-DR of each IT; and (iii) the FPN-counts relationship will be more linear for a shorter sub-DR. The basic logics manage to select an appropriate IT based on the background temperatures and the pixel-saturation situation (SAT = 0, or 1). IT (=16.6ms) operates for the sub-DR from -33~0 deg C; IT (=9ms) for the sub-DR from 0~35 deg C; IT (=5.2ms) for the sub-DR from 35~70 deg C, and IT (=2.5ms) for the situation that the target temperature is equal to or above 70 deg C.

The advanced logic functions in our DRM design have also been developed. The advanced logics, using some IT-prediction functions and using some feedback information from the outputs of Tracking and ATR (automatic target

recognition) functions, are designed in preventing the IT switching back and forth, and are useful in detecting and tracking weak targets in the counter-measurement (hot burning objects) situations. Here are some more detailed description for the advanced logics:

    (a). If the saturated pixels are from a target, the DRM will switch the IT to a shorter one to reduce the system sensitivity.

    (b). If the saturated pixels are from a clutter, or an uninteresting object, or a hot CM object, the DRM will not switch the IT.

    (c). The DRM estimates the IT_predict at which the target pixels will be saturated. If the IT to be switched to is larger than IT_predict, then the DRM will not switch the IT.

There is an additional advantage of our DRM design over the prior art. Since the DRM operates at several pre-. selected ITs, we know exactly the sensor's sensitivity and pixel saturation temperatures under different background temperatures based on our lab measurements. Therefore, we can estimate the seeker performance for target detection, recognition, and identification under different realistic conditions. The DRM's performances for target detection, recognition, and identification under different weather conditions have been estimated using the NVtherm tool from NVL. Several realistic examples have been included to show how well the DRM works.

## 2. MEASUREMENT RESULTS, REQUIREMENTS, AND PERFORMANCE CONSIDERATIONS

A CE (Cincinnati Electronics) *InSb* FPA's sensitivity has been estimated for ITs (integration times) ranging from 5.2ms to 16.6ms under different background temperatures from laboratory measurements. Based on the CE camera measurement data, the FPA NEDTs (noise equivalent delta temperatures) are calculated as shown in Figure 3. We then calculate the NEDTs for our seeker design based on the optical settings of our desgn and the opticals ettings of the CE camera. The NEDTs for our seeker design range from 10mk to 46mk spanning a temperature DR (dynamic range) from −30 to 70 deg C. Therefore, if we use ITs between 5.2ms and 16.6ms, we can meet both the requirements for sensitivity and DR.
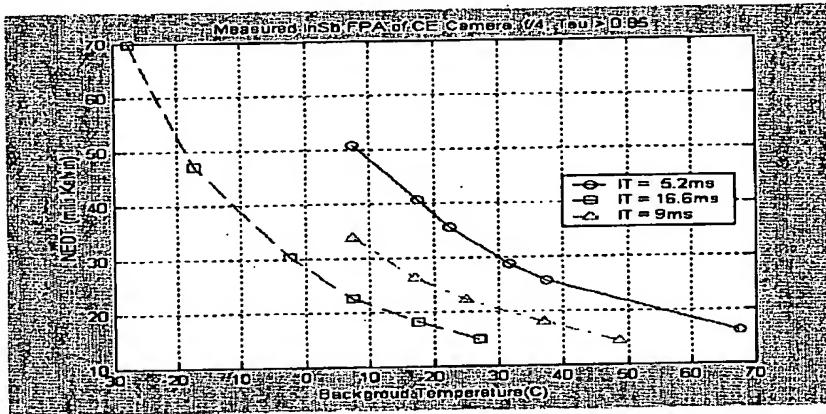


**Figure 3 NEDTs for the CE Camera**

1) Based on our laboratory measurements of the CE NC-256 Camera:
   For IT = 5.2ms, we know the dynamic range DR = 70 °C (from 0 °C to 70 °C) based on the CE camera manual and also our laboratory measurements.

   That is, for all the *ITs* ≤ *5.2 ms*, the requirement for $T_{max}$ can be satisfied.

2) FPA Sensitivity (NEDT):
   From Figure 3, for IT = 5.2ms, based on our laboratory measurements, we obtained that NEDT = 35.5mk (milli kelvin) at 22.5 °C & F = 4 (F is the lens f-number, F/4 is the number for the CE camera), and the optical transmittance Tau = 0.88.

3

For the same IT (= 5.2 ms), if we change the f-number F from 4 to 2.45, and change the Tau from 0.88 to 0.5, the NEDT will be reduced by a factor of $(4/2.45)^2 * 0.5/0.88$ (—= 1.56), i.e., NEDT = 22.8mk at 22.5 °C & F = 2.45 & Tau = 0.5.

That is, for all the *ITs ≥ 5.2 ms*, the NEDT can be satisfied.

3) For *InSb* FPAs, NEDT increases significantly at very low temperatures (e.g., -30 °C). That is, the FPA sensitivity is low at low temperatures. NEDT = 46mk at -28 deg C & (F = 2.45, Tau = 0.5).

## 3. OVERALL DESIGN CONSIDERATIONS AND DESCRIPTION

The design dilemma is that if we increase the system gain to meet the sensitivity requirement, the DR requirement may not be met, and vice versa. In this design, we divide the DR into three sub-DRs, and assign different ITs and electronic gains to the three specific sub-DRs. The purpose is to obtain as high as possible sensitivity for each sub-DRs, and still to be able to meet the minimum and maximum background temperature requirements. In addition, we select an IT = 2.5 ms when a very hot target is over 70 °C to avoid the target saturation. This IT (= 2.5 ms) is also selected when the missile has established trustable tracking and/or ATR, or when the missile is in the End-Game mode. In some NUC systems, the NUC is turned off during the End-Game mode since the system sensitivity will not be a problem at this mode. However, as discussed above, the secondary purpose of NUC is to reduce the high counts FPN artifacts to enhance tracking and ATR. In this design, by selecting a small IT, we can avoid the strong target saturation, and in the meanwhile, can still continue to operate the NUC function to suppress the FPN artifacts.

The selected ITs for the four sub-DRs are listed below:

1) For Target Temperatures > 70 deg (saturated target intensities) & Background Temperature: -10 ~ > 70 °C,
   IT = 2.5 ms.

2) For Background Temperature: 35 ~ 70 °C,
   IT = 5.2 ms.

3) For Background Temperature: 0 ~ 35 °C,
   IT = 9 ms.

4) For Background Temperature: -33 ~ 0 °C,
   IT = 16.6 ms.

## 4. DRM ALGORITHM DESCRIPTION

Four sub-DRs are selected using temperature units. Based on laboratory measurements for each individual FPA, each specific background temperature is related to a specific image mean (averaged) value in the unit of COUNTS. In this DRM algorithm, we measure and use the MIC (mean image count) to find out the operating sub-DR. For example, MIC_0_16[1] means the MIC at 0 °C & IT = 16.6 ms, and MIC_0_9 means the MIC at 0 °C & IT = 9 ms, etc. The MIC can be calculated from the center 64 x 64 elements of the FPA.

For adaptively switching sub-DRs to guarantee the target signatures to be within the linear dynamic range, it may be necessary to know whether there are saturated pixels caused by very hot targets or objects.

*SAT = 1*, if there are *M* pixels with values larger than 4050,
*SAT = 0*, otherwise[2].

---

[1] This value may be determined by laboratory measurements or factory calibrations.

[2] Under some situations, the saturated pixels may be from some uninterested objects or clutters and the signatures of a target may still be very weak. In these situations, we would like to keep the seeker in the high sensitivity mode, and thus a smarter algorithm is needed to know whether the saturation pixels are from a target or not.

$M$ is a selectable parameter (e.g., $2 \sim 3\%$ of the center 64 x 64 pixels). The saturation pixels can be estimated by a fast histogram method implementing in an FPGA[3]. An example using a MATLAB code to calculate the histogram of center 64 x 64 pixels is presented in the Appendix section.

There are some other conditions:

*Tracking* = *1*, if reliable tracking acquired,
*Tracking* = *0*, otherwise.


*ATR* = *1*, if reliable ATR acquired,
*ATR* = *0*, otherwise.

A saturation-related-integration-time-prediction (SRITP) function is included. The SRITP function is used when SAT = 0, and the DRM is going to change the current IT to a higher IT. This function predicts the IT that increases the system gain so that there are $M$ pixels with values larger than 4050 (i.e., SAT = 1). The DRM can then make an appropriate decision whether to change the IT or not by comparing the predicted IT with the IT to be changed to. This setting allows the DRM to work under a more steady state without switching the IT back and forth. An example using a MATLAB code to predict the IT is presented in the Appendix section.

In general, when the seeker starts to look, the system is still not quite under the stationary status and the targets may be quite far away from the seeker. Therefore, it is reasonable to start the NUC operation with the middle temperature sub-DR (we set the first 5 initial image frames at this mode). The detailed DRM algorithm is described below using a pseudo program code:

IT_number(1:4) = [2.5, 5.2, 9, 16.6];

% Initialization,
SubDR = 3;  % 1 for IT=2.5 ms, 2 for IT = 5.2 ms, 3 for IT=9 ms, and 4 for IT=16.6 ms

For 1 ≤ frame_number ≤ 5
   Set IT = 9 ms & GAIN_SEL = 0;  % 1 for high gain and 0 for low gain
   Low_bound = MIC_0_9;
   high_bound = MIC_35_9;
End

% Start the 6th frame,
For 5 < frame_number < $n$,

   If SAT = 0,
      IT_predict = SRITP(*CurrentFrame*, IT_number(SubDR), $M$);[4]
   End

   If MIC_cf < low_bound - B[5], and SubDR ≠ 4,   % MIC_cf is the current frame MIC

      SubDR = SubDR + 1;

      If SAT = 1, and (Tracking = 1 or ATR = 1),[6]

---

[3] During the NUC process, for the tracking mode, we can use the center 64 x 64 elements to compute the histogram. However, for the ATR mode, it may be advantageous to use the whole 256 x 256 elements. To reduce the computational intensity under this condition, we can under-sample the 256 x 256 image using every 4th or 8th pixel.
[4] This is the saturation related integration time prediction (SRITP) function.
[5] B is an adjustable buffering integer number, e.g., setting at 100. It prevents the integration times switch back and forth when the temperature during the flight is close to the two IT-switching temperatures (0°C and 35°C).

```
        SubDR = SubDR - 1;
    Else If SAT = 0, and IT_number(SubDR) > IT_predict, and (Tracking = 1 or ATR = 1), [7]
        SubDR = SubDR - 1;
    End

Else If MIC_cf > high_bound, and SubDR ≠ 1,
    SubDR = SubDR - 1;
Else If MIC_cf <high_bound, and SAT = 1, and (Tracking = 1 or ATR = 1), [8] and SubDR ≠ 1,
    SubDR = SubDR - 1;
End

If SubDR = 4, set IT=16.6ms; high_bound = MIC_0_16; end
If SubDR = 3, set IT=9ms; low_bound = MIC_0_9; high_bound = MIC_35_9; end
If SubDR = 2, set IT=5.2ms; low_bound = MIC_35_5; high_bound = MIC_70_5; end
If SubDR = 1, set IT=2.5ms; low_bound = MIC_70_2; end

End
```

The logics in the DRM algorithms from the above pseudo program code are illustrated using a block diagram in Figure 4. The logics are appropriately set to guarantee that the IT does not change more than one step up or down during one time frame. The two green boxes 'If MIC < low_bound' and 'If MIC_cf > high_bound' are the basic logics functions, which determine if the DRM stays at the current IT or switches to a lower or higher IT. The other three pink boxes are the advanced functions dealing with the IT prediction and pixel saturation situations. These advanced functions use the information fed back from the tracking and/or ATR functions. If the ATR or tracking are not available during the early tower test, just simply set ATR = 0, or tracking = 0. If both ATR and tracking are not available during the test, just set both ATR = 0 and tracking = 0. The DRM will use the basic logics functions. Therefore, in essence, the DRM with the basic logic functions is a feedforward system as already shown in Figure 2, while the DRM with the advanced logic functions is a feedback system as illustrated in Figure 5.

In summary, the DRM divides the required DR (-33 ~ 63 °C) into three sub-DRs by selecting three different ITs (5.2, 9, and 16.6 ms). With such an arrangement, the NUC system can meet both requirements for operating temperature dynamic range and system sensitivity. In addition, the DRM also select an IT (= 2.5 ms) to avoid pixel saturation for a very hot target (or a close target). With the additional information from conditions such as SAT, Tracking, and ATR, the DRM can adaptively select the appropriate ITs to guarantee that the target intensity is within the linear dynamic range, even for a very hot target. The maximum time for switching from the lowest temperature sub-DR to the highest temperature sub-DR (or vice versa) by the DRM is a sampling duration of three frames.

---

[6] For SAT = 1, if Tracking = 1 or ATR = 1, the DRM stays in the current sub-DR without changing the IT. However, if both Tracking = 0 and ATR = 0, then it is more likely that the saturated pixels are related to some uninterested objects, counter-measurement burning objects, or clutters. Therefore, the DRM switches to a higher IT for a higher sensitivity despite the pixel saturation situation.

[7] With this logic, the DRM predicts that if the IT changes to the next higher one then the next frame will be saturated, and that the IT will be changed back to the current IT at that frame. With this knowledge, the DRAM decides to stay in the current IT. This setting allows the DRM to work under a more steady state without flip-flopping the IT back and forth.

[8] On the other hand, if SAT = 1, but both Tracking = 0 and ATR = 0, then it is more likely that the saturated pixels are related to some uninterested objects, counter-measurement burning objects, or clutters. Therefore, the DRM stays in the higher sensitivity sub-DR to search for the weak target.
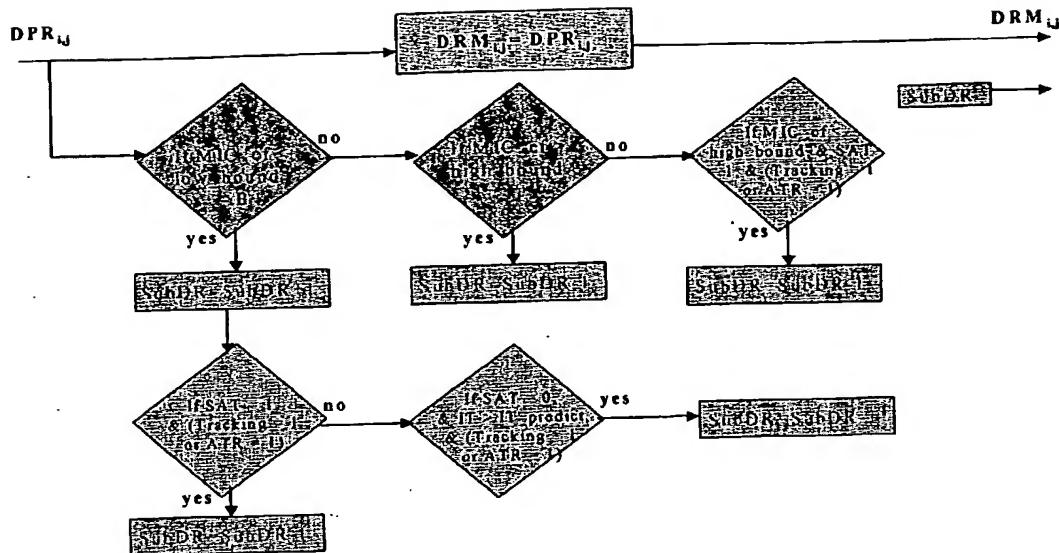
Figure 4 Logics of the DRM

Green Boxes: the basic logic functions; Pink Boxes: the advanced logic functions

DRM with the basic logics: a feedforward system;
DRM with the advanced logics: a feedback system
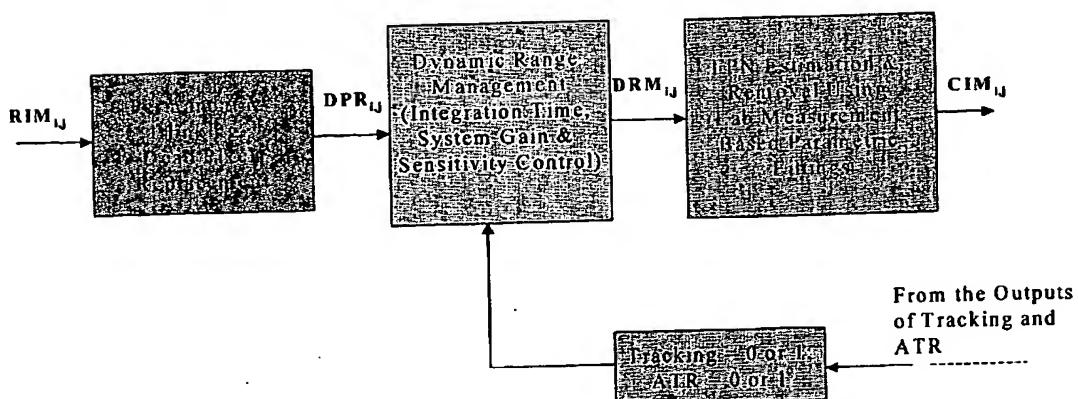


Figure 5 DRM with Advance Logic Functions

## 5. PERFORMANCE EVALUATION

The DRM's performance for target detection, recognition, and identification under different weather conditions have been estimated using the NVtherm tool from NVL. We also show several realistic examples to demonstrate how well the DRM works.

NVTherm is a PC based tool that can model staring thermal imagers with mid and far IR spectral bands (3 to 12 micrometer wavelength). We can input camera or seeker parameters and other optical design parameters to the

NVTherm tool to get the ranges for detection, recognition, and identification under different weather conditions and atmospheric transmission coefficients. For example, some critical parameters we can put into are: f/number, optical transmittance Tau, target size, Delta T, background contrast, FOV, integration times, D*, sensor type, sensor size, and weather conditions (Beer's law or Modtran model), etc.

# Target : a tank with a side view of 2.3 x 6.4 meters
# Delta T = 1.25 deg C



**Range vs. NEDT**
**Tau = 0.85**
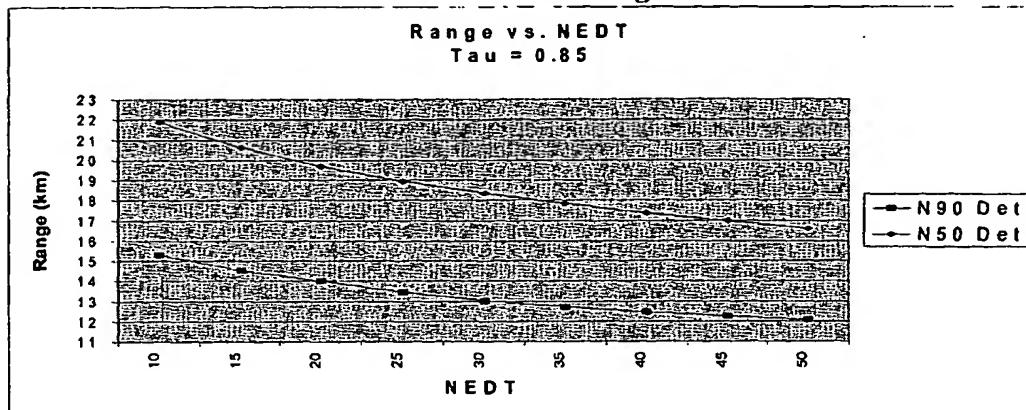
Figure 6 Performance of Target Detection



**Range vs. NEDT**
**Tau = 0.85**
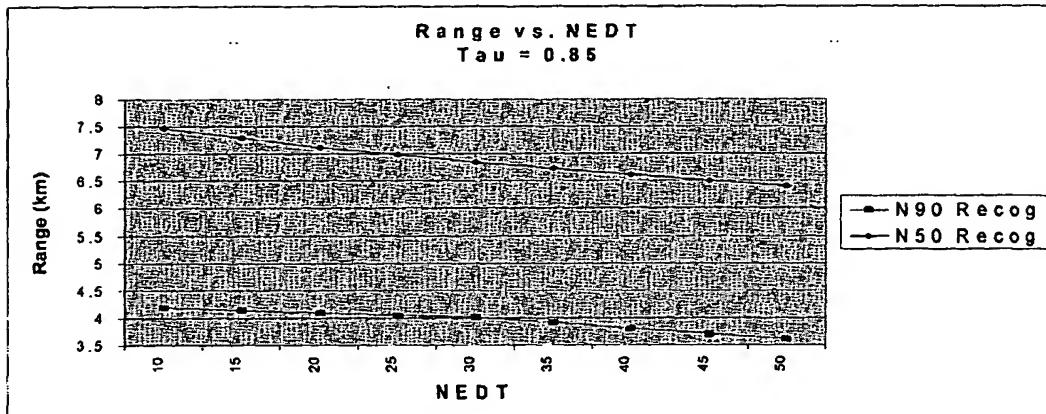
Figure 7 Performance of Target Recognition

In our NVTherm runs, we followed the target and weather models used by CE (Cincinnati Electronics), as indicated in the manual of the CE camera (with an *InSb* middle wavelength IR FPA). The *good* and *limited* atmospheric extinction coefficients are taken to be $\gamma$ = 0.2/km and $\gamma$ = 1/km respectively. Therefore, for good weather the atmospheric transmittance Tau = exp(-0.2) = 0.82, and for limited weather Tau = exp(-1) = 0.368. The standard target model for a tank's side view is 2.3 x 6.6 meters, and the tank target Delta T is 1.25 deg C. The N50 (50% probability target detection) criteria are 0.75 cycles for detection, 3 cycles for recognition, and 6 cycles for identification.

The performances for target detection, recognition, and identification as a function of sensor sensitivity (NEDT) under Good Weather Condition are shown in Figure 6, 7, and 8, respectively. Both N50 and N90 (90% probability target detection) results are presented. The N90 criteria would be more appropriate for our missile applications. The results

show that our DRM is working quite well under the good weather. For example, for a low sensitivity at NEDT = 50mk, we can start to detect the target at a range beyond 12 km, to recognize (tracking and ATR) the target at a range beyond 3.5 km.
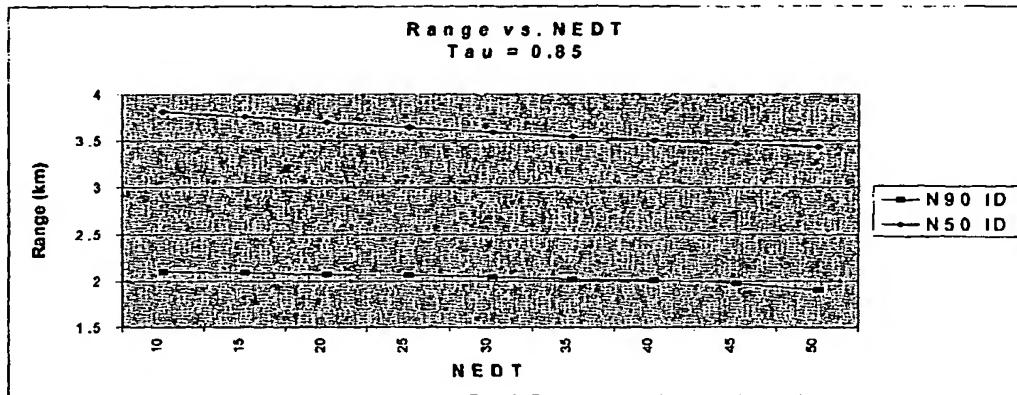


**Figure 8 Performance of Target Identification**
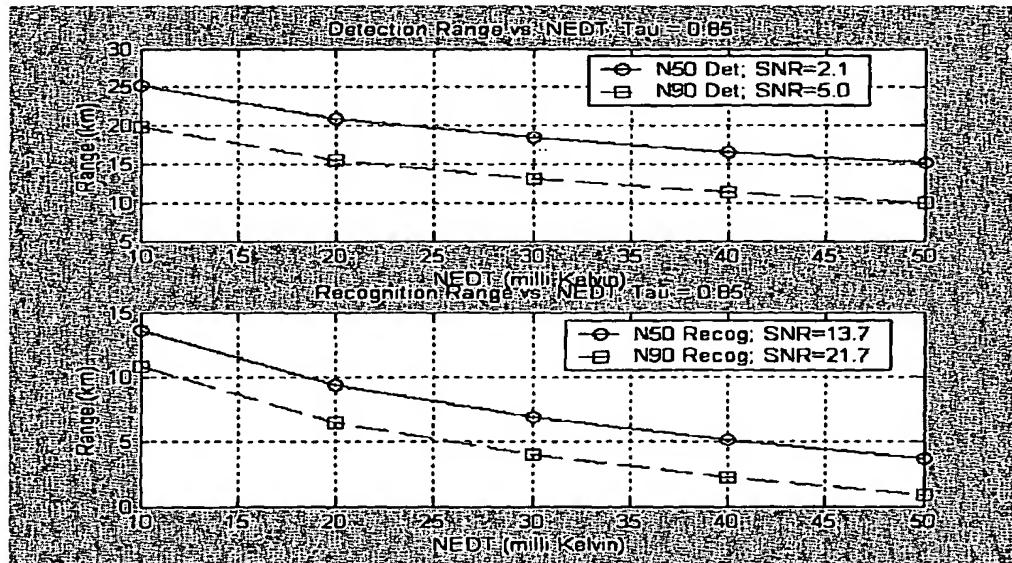


**Figure 9 Performance of Target Detection by Beer's Law using SNR Criteria**

The major reason we used the NVTherm for performance analysis is that it incorporates both the factors of system sensitivity and resolution. However, the N50 and N90 detection using Johnson's criteria are based on human eye's optical property. On the other hand, the missiles' detection generally use the CFAR (constant-false-alarm) thresholding technique, and thus the SNR criteria would be more appropriate for target detection in missile applications when operating within the range distance allowed by the optical resolution (i.e., for the longest operating range distance, the system MRT is still smaller or equal to 10 mk). The performance predictions for target detection and recognition by Beer's law using the SNR criteria are plotted in Figure 9, and these results are comparable to the results obtained by NVTherm shown in Figures 6 and 7.

For a specific sensor sensitivity (NEDT = 15~17mk), the performances predicted by the NVTherm for target detection, recognition, and identification under good and limited weather conditions are compared and the results are shown in Figure 10. It is seen that the bad weather can severely worsen the sensor performance. The N50 results for the CE camera are from the CE camera manual. They are plotted here to compare with the predicted N50 and N90 results of our optical settings.

## NEDT = 15~17 m k
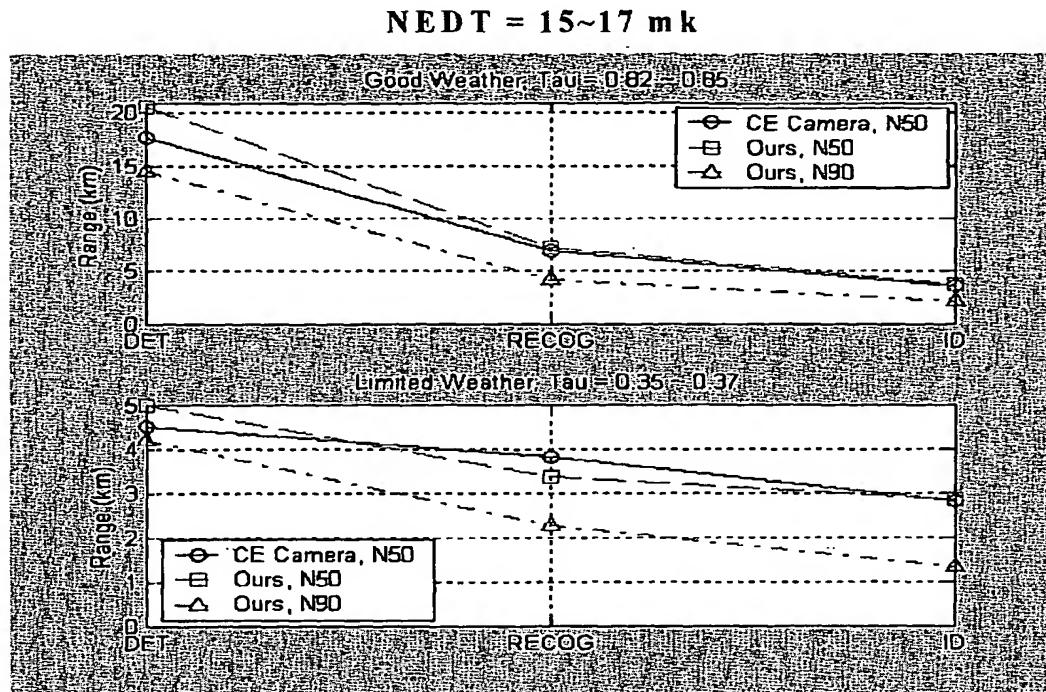


**Figure 10 Performances under Good and Limited Weather Conditions**

### 5.1 Low-temp Sub-DR Example

For a background temp –33 < Tb < 0 deg C, and for any target with temp[9] Tt < 30 deg C (the initial 5 time frames are set at IT = 9ms): the DRM will switch the IT from 9ms to 16.6ms at the 7th frame, and stay there until the missile hits the target.

In more detail, if Tb = -2.5 deg C, and the target is a tank with Tt = -1.25 deg C, then Delta T = 1.25 deg C, and NEDT = 20 mk. From Figures 6, 7, and 8, under a good weather condition, we can start to detection the target at about 14 km away, to recognize the target at about 4.1 km, and to identify the target at about 2.1 km.

### 5.2 Mid-temp Sub-DR Example

For a background temp 0 < Tb < 35 deg C, and for any target with temp Tt < 50 deg C (the initial 5 time frames are set at IT = 9ms): the DRM will set IT = 9ms at the 1st frame, and stay there until the missile hits the target.

---

[9] The temperatures Tb and Tt here are the apparent temperatures instead of the real temperatures. Please see Section 5.3 for the relationship between the apparent and the real temperatures.

In more detail, if Tb = 25 deg C, and the target is a tank with Tt = 26.25 deg C, then Delta T = 1.25 deg C, and NEDT = 15 mk. From Figure 10, under a good weather condition, we can start to detection the target at about 14.5 km away, to recognize the target at about 4.15 km, and to identify the target at about 2.1 km. However, under a limited weather condition, we can start to detection the target only at about 4.18km away, to recognize the target at about 2.25 km, and to identify the target at about 1.32 km.

## 5.3 Target Pixel-Saturation Examples

Based on the Beer-Lambert law:

$$T\_a = T\_r \cdot Tau^R, \qquad\qquad (1)$$

where $T\_a$ is the apparent target temperature at different ranges; $T\_r$ is the real target temperature; $R$ is the range. Then we have:

$$R = [log(T\_a) - log(T\_r)] / log(Tau) \qquad\qquad (2)$$

For a good weather ($Tau = 0.85$), if $T\_r = 65$ deg C, then $T\_a = 50$ deg C at a range
$R = 1.61$km, and $T\_a = 30$ deg C when $R = 4.76$km.

For a limited weather ($Tau = 0.35$), if $T\_r = 65$ deg C, then $T\_a = 50$ deg C at a range
$R = 0.25$km, and $T\_a = 30$ deg C when $R = 0.74$km.

For a scene with the background temp Tb = -2.5 deg C and the target *real* temp Tr = 65 deg C, under the good weather condition ($Tau = 0.85$):
The DRM will switch the IT from 9ms to 16.6ms at the 7th frame, and switch back to 9ms at $R = 4.76$km, and further switch to IT = 5.2ms at $R = 1.61$km. Then stay there until the missile hits the target.

## 5.4 CM (Burning Objects) Examples (CFT2 Data)

The CM (counter-measurement) example is from our recent captive-flight-test data. As shown in Figure 11, the pixels of the two burning objects are saturated at counts about 4075–4095 (12 bits images). That is, SAT = 1. However, the target signature is still quite weak at ranges longer than 2km. In this situation, we do not want to switch the IT to a shorter one, although SAT = 1.

For example, suppose Tb = 25 deg C, and Tt = 26.25 deg C, and the temperature of the two burning objects are above 100 deg C. Based on the DRM's advanced logic function: if tracking = 0 and ATR = 0, the DRM will stay at IT = 9ms with a high sensitivity (NEDT = 15mk) to detect and/or track the weak target.

## 6. SUMMARY

1). A CE *InSb* FPA's sensitivity has been measured and estimated. The NEDT ranges from 10 to 50mk spanning a temperature dynamic range from –30 to 70 deg C.

2). Four integration times (2.5, 5.2, 9, and 16.6 ms) have been selected for the DRM to meet the requirements for both the seeker sensitivity and temperature dynamic range.

3). The DRM's performances for target detection, recognition, and identification under different weather conditions have been estimated using the NVtherm tool. The results show that the performances are quite satisfactory.

4). The advanced logic functions developed for the DRM are helpful in preventing the IT switching back and forth and are useful in detecting and tracking weak targets in the counter-measurement (hot burning objects) situations.

R=3.62km          R=3.33km

R=2.15km          R=0.54km
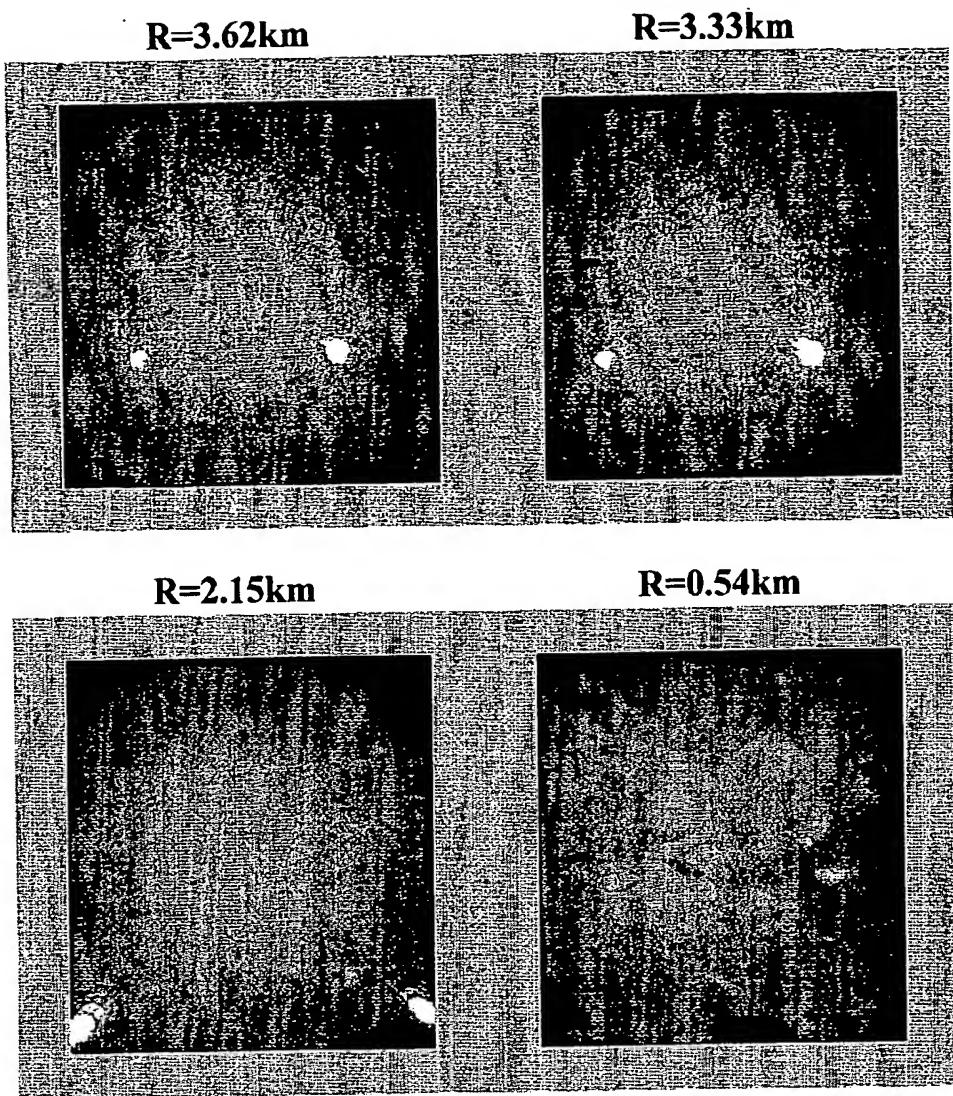
Figure 11 Counter-Measurement (Burning Object) Example from Captive Flight Test Data

12

1 CLAIMS

2     1.    A method to identify a potential target from image data

3 representing a scene, comprising:

4     performing at least one of a pre-detection temporal fusion and a pre-

5 detection spatial fusion of the image data; and

6     thresholding the image data after performing the step of performing.

7

8     2.    The method of claim 1, wherein:

9     performing the pre-detection temporal fusion comprises temporally

10 integrating the image data from a particular sensor across a plurality of time

11 frames; and

12     performing the pre-detection spatial fusion comprises fusing the image

13 data from a plurality of sensors across a single time frame.

14

15     3.    The method of claim 1, wherein the pre-detection temporal fusion

16 and the pre-detection spatial fusion includes at least one of an additive fusion,

17 multiplicative fusion, MIN fusion, and MAX fusion.

18

4

1     4.    The method of claim 1, wherein the thresholding includes at least

2    one of:

3     a double-thresholding wherein an upper and a lower bound thresholds

4    are set to identify the potential target; and

5     a reverse-thresholding wherein a potential target identification level is set

6    to be below a particular threshold.

7

8     5.    A method to identify a potential target from image data of a scene,

9    comprising:

10     thresholding the image data from across multiple time frames or

11    multiple sensor platforms; and

12     fusing the image data after performing the thresholding.

13

14     6.    The method of claim 5, wherein the thresholding includes at least

15    one of:

16     double-thresholding the image data, wherein an upper and a lower

17    bound threshold are set to identify the potential target; and

18     reverse-thresholding wherein a potential target identification level is set

19    to be below a particular threshold.

20

21     7.    The method of claims 1 or 5, wherein said step of thresholding

22    produces thresholded image data, the method further comprising:

23     identifying candidate targets from the thresholded image data.

1

2     8.    A   device   to   identify   potential   targets   from   image   data

3  representative of a scene, comprising:

4        a fusion module configured to perform at least one of integrating the

5  image data across a plurality of time frames and integrating a plurality of

6  images in a single time frame; and

7        a threshold module configured to apply thresholding techniques on the

8  image data.

9

10     9.    The device of claim 8 wherein said device further includes at least

11  one sensor configured to sense the scene across the plurality of time frames.

12

13     10.    The device of claim 8, wherein fusion module is configured to

14  perform at least one of an additive fusion, multiplicative fusion, MIN fusion,

15  and MAX fusion.

16

17     11.    The device of claim 8, wherein the fusion module is configured to

18  perform at least one of a pre-detection fusion and a persistence test.

19

20     12.    The device of claim 8, wherein the threshold module is configured

21  to perform at least one of a double-thresholding technique and a reverse-

22  thresholding technique.

6

4358-0113 Provisional

## ABSTRACT

It is advantageous to identify potential targets as far away as possible. For a simple background scene such as a blue sky, a target may be recognized from a relatively long range distance. However, for some high clutter situations

5 such as maintains and cities, the detection range is severely reduced. Moreover, clutter situation are often complicated. Also the background clutter may be non-stationary. In these types of situations, the traditional constant false alarm ratio (CFAR) detection technique often fails. To solve the problems discussed above, spatio-temporal fusion or integrating may be used to enhance

10 potential target recognition. Also, detection schemes, such as double-thresholding and reverse-thresholding techniques, may be applied to further enhance potential target recognition.

100



FIG. 1A

4358 - 0113   Provisional



SENSOR(S)

THRESHOLD MODULE
Double Threshold
Reverse Threshold

FUSION MODULE
Temporal
Spatial
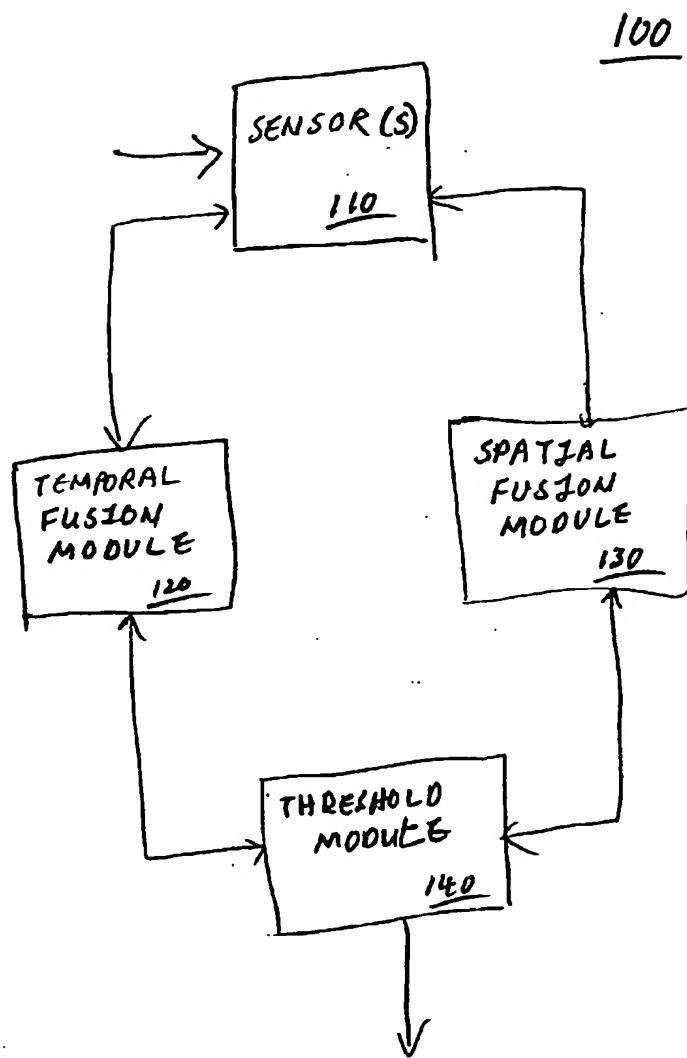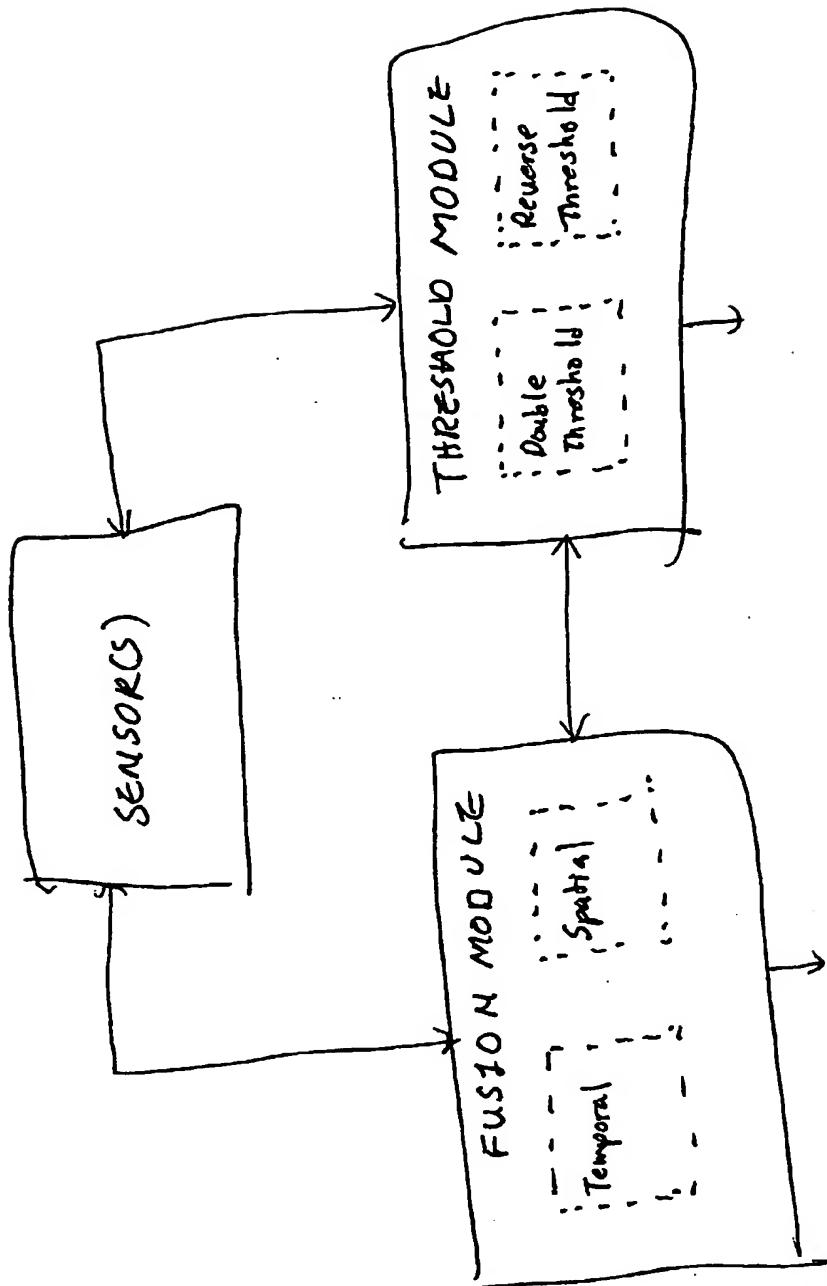
# Document made available under the Patent Cooperation Treaty (PCT)

International application number: PCT/US04/008345

International filing date: 18 March 2004 (18.03.2004)

Document type: Certified copy of priority document

Document details: Country/Office: US
Number: 60/456,190
Filing date: 21 March 2003 (21.03.2003)

Date of receipt at the International Bureau: 23 December 2004 (23.12.2004)

Remark: Priority document submitted or transmitted to the International Bureau in compliance with Rule 17.1(a) or (b)